PHYSICAL REVIEW B **103**, 174413 (2021)

Stacking faults in α-RuCl$_3$ revealed by local electric polarization

Xinrun Mi,[1,*] Xiao Wang,[2,*] Hengrui Gui,[1] Maocai Pi,[1] Tingting Zheng,[1] Kunya Yang,[1] Yuhan Gan,[1] Peipei Wang,[3] Alei Li,[3] Aifeng Wang,[1] Liyuan Zhang,[3] Yixi Su,[2] Yisheng Chai,[1] and Mingquan He[1,†]

[1]*Low Temperature Physics Laboratory, College of Physics & Center of Quantum Materials and Devices, Chongqing University, Chongqing 401331, China*

[2]*Jülich Centre for Neutron Science (JCNS) at Heinz Maier-Leibnitz Zentrum (MLZ), Forschungszentrum Jülich GmbH, Lichtenbergstrasse 1, D-85747 Garching, Germany*

[3]*Department of Physics, Southern University of Science and Technology, Shenzhen 518055, China*

(Received 15 January 2021; revised 21 April 2021; accepted 27 April 2021; published 11 May 2021)

We present out-of-plane dielectric and magnetodielectric measurements of single-crystalline α-RuCl$_3$ with various degrees of stacking faults. A frequency-dependent, but field-independent, dielectric anomaly appears at $T_A(f = 100\text{ kHz}) \sim 4$ K once both magnetic transitions at $T_{N1} \sim 7$ K and $T_{N2} \sim 14$ K set in. The observed dielectric anomaly is attributed to the emergence of possible local electric polarizations whose inversion symmetry is broken by inhomogeneously distributed stacking faults. A field-induced intermediate phase is only observed when a magnetic field is applied perpendicular to the Ru-Ru bonds for samples with minimal stacking faults. Less pronounced in-plane anisotropy is found in samples with a sizable contribution from stacking imperfections. Our findings suggest that dielectric measurement is a sensitive probe in detecting the structural and magnetic properties, which may be a promising tool, especially in studying α-RuCl$_3$ thin-film devices. Moreover, the stacking details of RuCl$_3$ layers strongly affect the ground state both in the magnetic and electric channels. Such a fragile ground state against stacking faults needs to be overcome for realistic applications utilizing the magnetic and/or electric properties of Kitaev-based physics in α-RuCl$_3$.

DOI: 10.1103/PhysRevB.103.174413

I. INTRODUCTION

The possible emergence of Majorana fermion excitations in an $S = 1/2$ Kitaev quantum spin-liquid (QSL) state is thought to be a promising channel to realize topological quantum computing [1,2]. The solvability of the honeycomb Kitaev model has boosted experimental interests to search for real materials in which Kitaev physics is at play. Some Mott insulators with strong spin-orbit coupling-induced effective spin-1/2 ($J_{\text{eff}} = 1/2$) appear to be promising candidates for Kitaev materials [3–5]. To date, a few possible compounds including iridates (A_2IrO$_3$, A = Li, Na) [6–11] and ruthenates (α-RuCl$_3$) [12–22] have been found, although conclusive evidence is still lacking.

Of particular interest is the layered compound α-RuCl$_3$, which is in close proximity to the ideal Kitaev model although a zigzag antiferromagnetic (AF) order is favored at low temperatures due to sizable Heisenberg interactions and nonzero off-diagonal terms [4,12,23,24]. The AF ground state is unstable against the application of pressure [18,25,26] and in-plane magnetic fields [19,27–31]. The system enters a quantum disordered phase when an in-plane magnetic field higher than a critical value of $\mu_0 H_c \sim 8$ T is applied. Evidence of fractional excitations emerging from this field-induced quantum disordered state has been reported by various techniques [22,27,32], but the nature of this phase is still under debate. Meanwhile, the magnetic transition is very sensitive to the stacking sequence of the honeycomb layers. It has been suggested that a stacking of *ABC* series produces the AF transition at $T_{N1} \sim 7$ K, and that an *ABAB* stacking is responsible for the transition at $T_{N2} \sim 14$ K [13]. Neutron scattering experiments indeed found non-negligible interlayer magnetic interactions [29,33], which necessarily couple to the details of layer stacking. Stacking faults can be easily formed due to weak interlayer van der Waals bonding (<1 meV [34]) and the small energy difference between these two configurations. The formation of stacking faults has been evidenced by the appearance of multiple magnetic transitions within one sample [13,16]. To date, much progress has been made to unravel the interplay between magnetic, lattice, and Kitaev interactions both theoretically and experimentally. However, less effort has been applied to the study of stacking faults and their related magnetic properties from the charge and/or electric degrees of freedom, which are also important aspects to understand the ground state and for future real device applications.

In this paper, we report on the out-of-plane dielectric and magnetodielectric measurements of α-RuCl$_3$ single crystals with different degrees of stacking faults. A frequency-dependent dielectric anomaly is observed at $T_A(f = 100\text{ kHz}) \sim 4$ K in samples showing both magnetic transitions at $T_{N1} \sim 7$ K and $T_{N2} \sim 14$ K. Suppression of the magnetic transitions using in-plane magnetic fields produces a negligible effect on the observed dielectric anomaly. No signature of such a dielectric anomaly is found in crystals

---

[*] These authors contributed equally to this work.

[†] mingquan.he@cqu.edu.cn

with a dominant transition at $T_{N1} \sim 7$ K. We conclude that the observed dielectric anomaly likely originates from local electric polarizations, which appear at the interfaces between *ABC* and *ABAB* stacking. The inversion symmetry is possibly broken by the inhomogeneous distribution of stacking faults. The magnetodielectric effect is found to be anisotropic for in-plane magnetic fields applied parallel and perpendicular to the Ru-Ru bonds. The field-induced intermediate state found in earlier reports with magnetic fields applied perpendicular to the Ru-Ru bonds [29,33], is confirmed by our magnetodielectric measurements for samples with minimal stacking faults. Our results suggest that the complex magnetic phases in α-RuCl$_3$ can also be accessed by a dielectric probe, and that the structural details determine the ground state in both the magnetic and electric channels.

II. METHODS

α-RuCl$_3$ single crystals were grown by the chemical vapor transport method in a two-zone furnace. Commercial RuCl$_3$ powders (3 g in mass, Furuya metal) were first sealed in a quartz tube (length: 12 cm; diameter: 2 cm) and then put in a two-zone furnace (source temperature 790 °C, sink temperature 710 °C). Black shiny plates of α-RuCl$_3$ single crystals would appear at the sink end after dwelling for 5 days. The samples used in this study have a typical dimension of $5 \times 5 \times 0.3\,\mathrm{mm}^3$. The dielectric constant of the α-RuCl$_3$ single crystals was measured by an Agilent E4980A *LCR* meter with electric field applied perpendicular to the *ab* plane ($\mathbf{E} \parallel c$ in the $R\bar{3}$ notation) in a 9-T Quantum Design DynaCool system and a 14-T Oxford cryostat. The electrodes were prepared by sputtering 50-nm Au on both sides of the *ab* crystal surfaces. The heat capacity measurements were performed in a 9-T Quantum Design DynaCool system.

III. RESULTS AND DISCUSSIONS

A. Structural and magnetic transitions

The normalized dielectric constants, $\varepsilon(T)/\varepsilon_{300\,\mathrm{K}}$, of three typical α-RuCl$_3$ single crystals measured at zero magnetic field are presented in Figs. 1(a)–1(c). The electric field was applied perpendicular to the *ab* plane ($\mathbf{E} \parallel c \perp ab$). The room-temperature relative dielectric constant, $\varepsilon_r(300\text{ K}) = \varepsilon/\varepsilon_0 = Cd/\varepsilon_0 A$, was estimated to be ~15 for all three samples. Here, ε_0 is the dielectric constant of vacuum, C is the measured capacitance, d is the sample thickness, and A is the effective area of the electrodes deposited on the sample surfaces. Hysteretic steplike features appearing at T_{sc} (upon cooling) and T_{sw} (upon warming) are clearly seen in all samples, which are signatures of a first-order structural transition. Evidence of such a structural transition has also been captured by other techniques, including heat capacity [35], magnetization [16], x ray [17], Raman scattering [14], thermal expansion [26,28,35,36], and an earlier dielectric study [37]. Instead of the high-temperature monoclinic $C2/m$ structure, it is likely that a different phase is formed at low temperatures (a trigonal $P3_112$ or rhombohedral $R\bar{3}$ phase [17,31,38]). However, the origin of this structural transition remains unclear. Here, we adopt the $R\bar{3}$ convention for convenience. Given the nature of weak van der Waals bonding, the formation of stacking faults is inevitable during such a hysteretic transition. Only one dominant magnetic transition occurring at either $T_{N1} \sim 7$ K or $T_{N2} \sim 14$ K would be expected if a crystal has minimal stacking faults. As shown in Fig. 1(d), this case is realized in sample 1 which shows a dominant sharp peak at $T_{N1} = 7.3$ K in the specific heat data. For samples 2 and 3, another steplike feature appears at $T_{N2} = 14$ K in addition to the major peak located at T_{N1} [see Figs. 1(e) and 1(f)]. This simply indicates a considerable mixing of *ABC* and *ABAB* polymorphs and sizable stacking faults [13]. Different degrees of stacking faults in the three samples studied here are likely caused by careless handling during the preparation of the electrodes [13]. Note that a broad hump sitting around 10 K is also visible in sample 3. A similar feature has been reported earlier [16,21,26], whose origin is attributed to competing exchange interactions [16]. Although the exact nature is yet to be clarified, sizable stacking faults certainly play an important role.

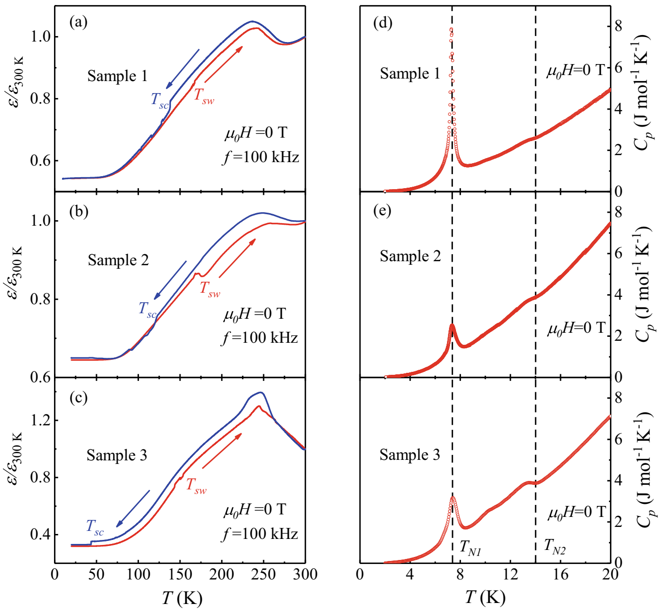

FIG. 1. (a)–(c) Temperature dependence of the normalized dielectric constant, $\varepsilon(T)/\varepsilon_{300\,\mathrm{K}}$, measured at zero field for three typical samples. The electric field was applied perpendicular to the *ab* plane ($\mathbf{E} \,||\, c \perp ab$ in the $R\bar{3}$ representation). A sample-dependent hysteretic structural transition is observed in all three samples using a temperature ramping rate of 1 K/min (T_{sc}: transition temperature for cooling; T_{sw}: transition temperature upon warming). (d)–(f) Temperature evolution of specific heat near the magnetic transitions for the three corresponding samples. Vertical dashed lines in (d)–(f) mark the magnetic transitions.

The width of the hysteretic structural transition $T_{s,\mathrm{width}} = T_{sw} - T_{sc}$, also correlates with the degree of stacking faults. Compared to sample 1, more and more stacking faults are introduced into samples 2 and 3 as evidenced by the heat capacity results. Correspondingly, $T_{s,\mathrm{width}}$ spans over a larger and larger temperature range for samples 2 and 3. It is likely that when cooled below T_{sc}, the transformation between the high-temperature and low-temperature phases is less complete for samples 2 and 3 than for sample 1 [26,36]. Naturally, more stacking faults are formed and a larger hysteresis is necessary to restore the high-temperature structure upon warming. Note

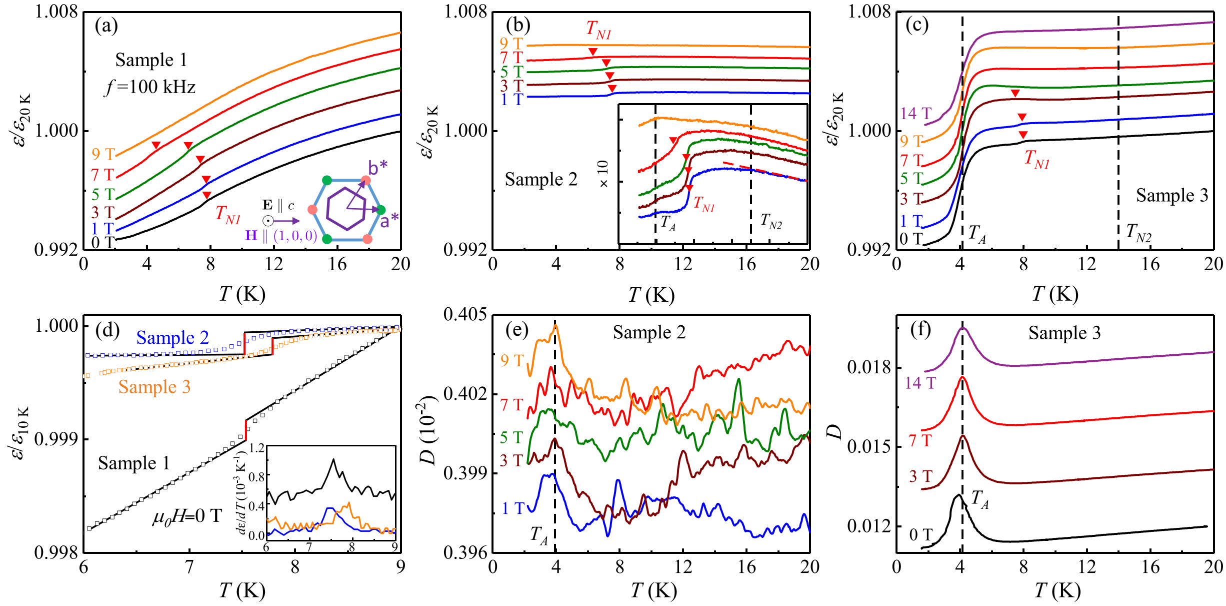

FIG. 2. (a)–(c) Temperature evolution of $\varepsilon/\varepsilon_{20\ \mathrm{K}}$, recorded at $f = 100$ kHz. In-plane magnetic fields were applied along the reciprocal space (1,0, 0) direction [parallel to the real-space Ru-Ru bonds; see the inset in (a)]. Curves have been shifted vertically for clarity. (d) The enlarged view of $\varepsilon/\varepsilon_{10\ \mathrm{K}}$ near T_{N1}. The open squares are experimental raw data and the lines are guides to the eyes. The inset of (d) shows $d\varepsilon/dT$. (e) and (f) The dissipation (D) as a function of temperature measured in fixed fields of samples 2 and 3, respectively. Inset in (a): An illustration of the in-plane reciprocal space (inner purple hexagon) and real space (outer blue hexagon) representations. Solid triangles in (a)–(c) track the variation of T_{N1} with respect to in-plane magnetic fields. Vertical dashed lines in (b) and (c) mark the dielectric anomaly and the transition at T_{N2} [determined by the specific heat data in Figs. 1(e) and 1(f)].

that the dielectric constant is generally not fully recovered after T_{sw} upon warming, although the lattice constants are more or less restored [26,28,35,36]. This implies that the formed stacking faults are irreversible when passing through the structural transition, and that dielectric probing is sensitive to these minute structural perturbations. A reversible dielectric constant is eventually achieved near room temperature when the thermal energy is strong enough to wipe out these tiny structural differences.

B. Dielectric anomaly

In Fig. 2, we present the temperature dependence of the normalized dielectric constant $\varepsilon/\varepsilon_{20\ \mathrm{K}}$ near the AF transition region. The magnetic fields were applied along the Ru-Ru bonds [$\mathbf{H} \parallel (1,0,0)$ in reciprocal space; see the inset of Fig. 2(a)]. No significant differences are found when applying magnetic fields perpendicular to the Ru-Ru bonds for a temperature sweep (data not shown here). Clearly, these three samples have a different dielectric response with respect to temperatures and external in-plane magnetic fields. The $\varepsilon/\varepsilon_{20\ \mathrm{K}}$ of sample 1 decreases continuously with cooling in all fields [Fig. 2(a)]. At zero field, only a steplike jump appears at $T_{N1} = 7.5$ K [determined by the peak in $d\varepsilon/dT$; see the inset of Fig. 2(d)], below which the dielectric constant is slightly reduced. This magnetic-order-induced dielectric reduction is a possible signature of a type-II multiferroic as discussed by Zheng *et al.* [37]. Another more trivial explanation could be a simple enhancement of the c-axis lattice constant caused by magnetoelastic coupling as found by thermal-expansion measurements [26,28]. Upon application of in-plane magnetic fields, the AF transition at T_{N1} shifts gradually towards lower temperatures and eventually vanishes above the critical field $\mu_0 H_{c1} \sim 8$ T. Suppression of T_{N1} by in-plane magnetic fields has also been detected by other techniques, which is thought to be a prominent way for driving the system into the QSL state [19,27–31].

In contrast to sample 1, a negative linear slope is found in sample 2 [see the inset of Fig. 2(b)] when cooled down from 20 K. This linear temperature dependence deviates below $T_{N2} \sim 14$ K, indicating the appearance of the AF order in the *ABAB* polymorph. Further cooling leads to a steplike jump at $T_{N1} = 7.5$ K in small fields. Note that the size of the dielectric reduction occurring at T_{N1} is similar in all three samples, as shown in Fig. 2(d), but the transition appears to be sharpest in sample 1, as expected [see the inset of Fig. 2(d)]. In addition to the magnetic transitions, a dielectric anomaly emerges at a lower temperature $T_A \sim 4$ K for $f = 100$ kHz, which is absent in sample 1. As illustrated in Fig. 2(e), this dielectric anomaly is accompanied by a sizable dissipation, and T_A is defined as the temperature where the dissipation shows a peak. The dielectric anomaly becomes less visible in the intermediate field region (about 5–7 T) as T_{N1} is pushed gradually towards T_A. However, a clear signature is recovered again at $\mu_0 H = 9$ T once the AF order formed below T_{N1} is fully suppressed. The dissipation peak [Fig. 2(e)], however, stays nearly intact throughout the studied field range. This implies little effect on the dielectric anomaly by applying in-plane magnetic fields.

The dielectric anomaly becomes the dominant feature in sample 3 [Fig. 2(c)], and a significant amount of dielectric constant is lost at T_A. A clear peak is seen in the dissipation at T_A, as shown in Fig. 2(f), which is field independent up

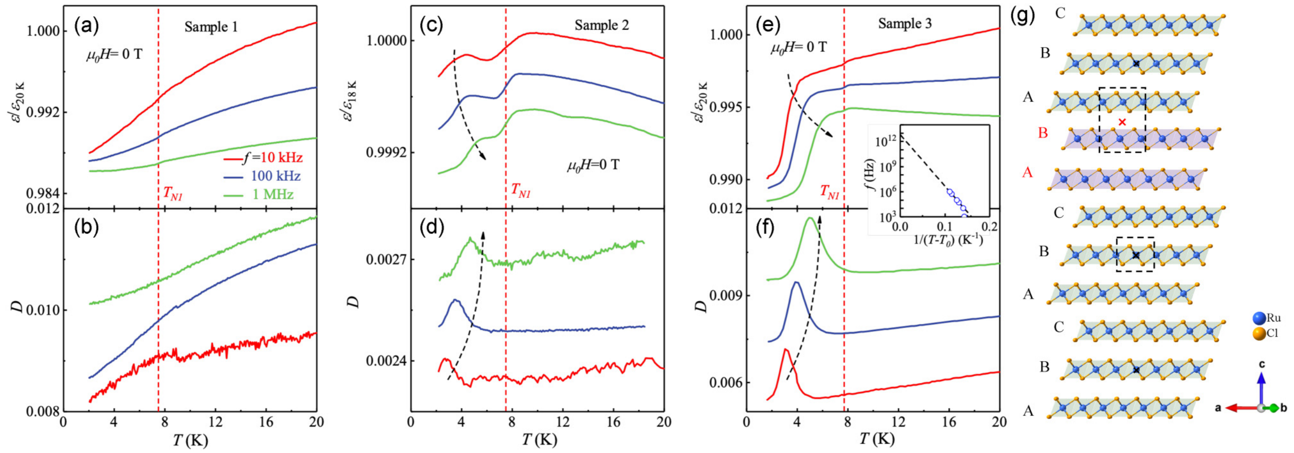

FIG. 3. Frequency dependence of (a), (c), (e) $\varepsilon/\varepsilon_{20\,\mathrm{K}}$ and (b), (d), (f) the corresponding dissipation (D) of all samples measured in zero field. The dielectric anomaly depends strongly on frequency and T_A shifts gradually to higher temperatures for increasing frequency. (g) A schematic illustration of inversion symmetry breaking caused by nonuniformly distributed stacking faults. The black (red) cross marked out by a dashed rectangle labels the inversion center of each *ABC* (*AB*) unit. The inversion counterpart is missing for the bottom *ABC* segment when an *AB* unit is inserted asymmetrically. The inset in (e) and (f) is a fitting of the frequency dependence of T_A according to the Vogel-Fulcher law $f = f_0 \exp[-E/k_B(T_A - T_0)]$ using the Boltzmann constant k_B, a temperature constant $T_0 = -4$ K, an activation energy $E = 143$ K, and a characteristic frequency $f_0 = 7.6 \times 10^{12}$ Hz.

to 14 T. As indicated by the specific heat data (see Fig. 1), samples 2 and 3 have a higher degree of stacking faults. Thus, the observed dielectric anomaly correlates strongly with the degree of stacking faults. An earlier study performed by Aoyama *et al.* [39] reported such a dielectric anomaly for both $\mathbf{E} \parallel c$ and $\mathbf{E} \parallel ab$ in samples with a major transition at $T_{N2} \sim 14$ K. On the other hand, Zheng *et al.* [37] only found a steplike dielectric reduction at $T_{N1} \sim 7$ K for $\mathbf{E} \parallel c$ in samples with minimal stacking faults. Aoyama *et al.* [39] suggested that zigzag AF order-induced local polarizations are responsible for the observed dielectric anomaly in the case of $\mathbf{E} \parallel ab$. However, unlike the AF transitions which fade away above $\mu_0H_{c2} \sim 10$ T [see Refs. [16,39] and Figs. 4(e) and 4(f)], the observed dielectric anomaly for $\mathbf{E} \parallel c$ appears to be robust up to 14 T, as shown in Figs. 2(c) and 2(f). Moreover, the dielectric loss for $\mathbf{E} \parallel c$ below T_A is much more profound in sample 3 (about 5×10^{-3}) than that of crystals with less stacking faults (negligible dielectric loss in samples 1 and 2, $\sim 5 \times 10^{-4}$ dielectric loss in samples with dominant *ABAB* stacking [39]). Therefore, it is likely that the dielectric anomaly found here for $\mathbf{E} \parallel c$ is more closely associated with stacking faults than the zigzag AF order.

To further unravel the nature of the observed dielectric anomaly, its frequency dependence is explored in Fig. 3. Clearly, the dielectric anomaly is strongly frequency dependent. As shown in Figs. 3(c)–3(f), T_A moves monotonically towards higher temperatures for increasing frequency. Therefore, any long-range order can be ruled out, as no frequency dependence would be expected. A similar frequency dependence of the dielectric anomaly is also found for $\mathbf{E} \parallel ab$, and its origin is attributed to a glassy state of zigzag AF order-induced local electric polarizations [39]. As displayed in the inset of Figs. 3(c) and 3(f), the frequency dependence of T_A can be well described by the Vogel-Fulcher law $f = f_0 \exp[-E/k_B(T_A - T_0)]$ with similar $T_0 = -4$ K, activation energy $E = 143$ K, and characteristic frequency $f_0 = 7.6 \times 10^{12}$ Hz compared to those of $\mathbf{E} \parallel ab$ [39]. This suggests that the same physics is at play for both $\mathbf{E} \parallel ab$ and $\mathbf{E} \parallel c$, i.e., a possible glassy state of local electric polarizations is formed. Such an argument is plausible as the characteristics of dipolar glasses [40], spin glasses [41], and relaxor ferroelectrics [42] can be described by a similar phenomenological Vogel-Fulcher approach. Given the negligible response to in-plane magnetic fields, the electric polarizations here for $\mathbf{E} \parallel c$ are most probably caused by stacking faults located at the *ABC*/*ABAB* interfaces. As sketched in Fig. 3(g), the inversion center sits in the middle of the *B* layer in each *ABC* unit of pure *ABC* stacking. The bottom *ABC* segment could not find its inversion counterpart if an *AB* unit was inserted asymmetrically into *ABC* layers. We note that a uniform distribution of stacking faults still preserves the inversion symmetry. Instead of zigzag AF order-induced symmetry breaking in the *ab* plane, here along the *c* axis, the inversion symmetry is broken locally by inhomogeneously distributed stacking faults.

C. Magnetodielectric effect and field-induced intermediate state

In this section, we study the anisotropic magnetodielectric effect and the results are presented in Fig. 4. In-plane anisotropy and multiple field-induced magnetic phase transitions are clearly seen in all samples. In the paramagnetic state above T_{N1} or T_{N2}, the magnetodielectric data generally show temperature-independent backgrounds, which vary between samples and field directions. This discrepancy might be caused by sample and thermal history-dependent stacking faults as measurements for different field orientations were performed after several thermal cycles up to room temperature.

For sample 1 shown in Figs. 4(a) and 4(b), a local minimum at $\mu_0H_r \sim 4$ T is observed consistently below T_{N1} along both field directions. This dip feature is likely associated with the

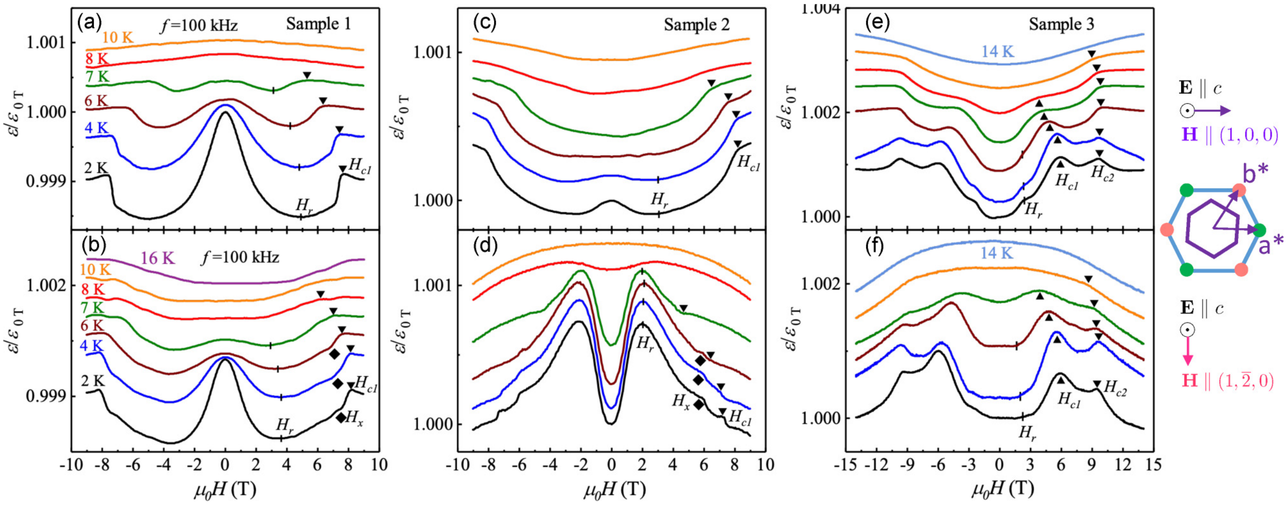

FIG. 4. Magnetodielectric effect measured at fixed temperatures and constant frequency $f = 100$ kHz. In (a) and (b), magnetic fields were along and perpendicular to the Ru-Ru bonds with $\mathbf{H} \parallel (1, 0, 0)$ and $\mathbf{H} \parallel (1, \bar{2}, 0)$, respectively, for sample 1. (c), (d) and (e), (f) Same measurements with (a) and (b) for samples 2 and 3, respectively. Curves are shifted vertically for clarity.

domain repopulation as found by neutron scattering experiments [43]. The domain reorientation apparently exists in all samples. The transition from the AF ordered state to the quantum disordered phase is evidenced by a steplike jump sitting at $\mu_0 H_{c1} \sim 8$ T in samples 1 and 2. Additionally, a small bump is found at $\mu_0 H_x \sim 6$ T for $\mathbf{H} \parallel (1, \bar{2}, 0)$ only (perpendicular to the Ru-Ru bonds), which is more pronounced in sample 2 [see Fig. 4(d)]. This field-induced intermediate phase between H_x and H_{c1} with field applied perpendicular to the Ru-Ru bonds has also been evidenced by AC susceptibility and inelastic neutron scattering experiments [29,33], although its origin still remains elusive.

Figures 4(e) and 4(f) display the results of sample 3. An additional peak appears at $\mu_0 H_{c2} \sim 10$ T below T_{N2}, apart from the familiar features at $\mu_0 H_r$ and $\mu_0 H_{c1}$. Apparently, a higher field is necessary to partially align the zigzag order emerging below T_{N2} [16,39]. Compared to the other two samples, the critical field $\mu_0 H_{c1}$ for suppressing the AF zigzag order formed below T_{N1} is reduced from ~8 to ~6 T at 2 K. The field-induced intermediate phase is not visible in sample 3 due to the close proximity between $\mu_0 H_{c1}$ and $\mu_0 H_x$.

D. Phase diagram

In Fig. 5, we summarize the T-H phase diagrams of the three different samples studied here. The data points were extracted from the dielectric, magnetodielectric, and specific heat results. One sees that all the phases found by other

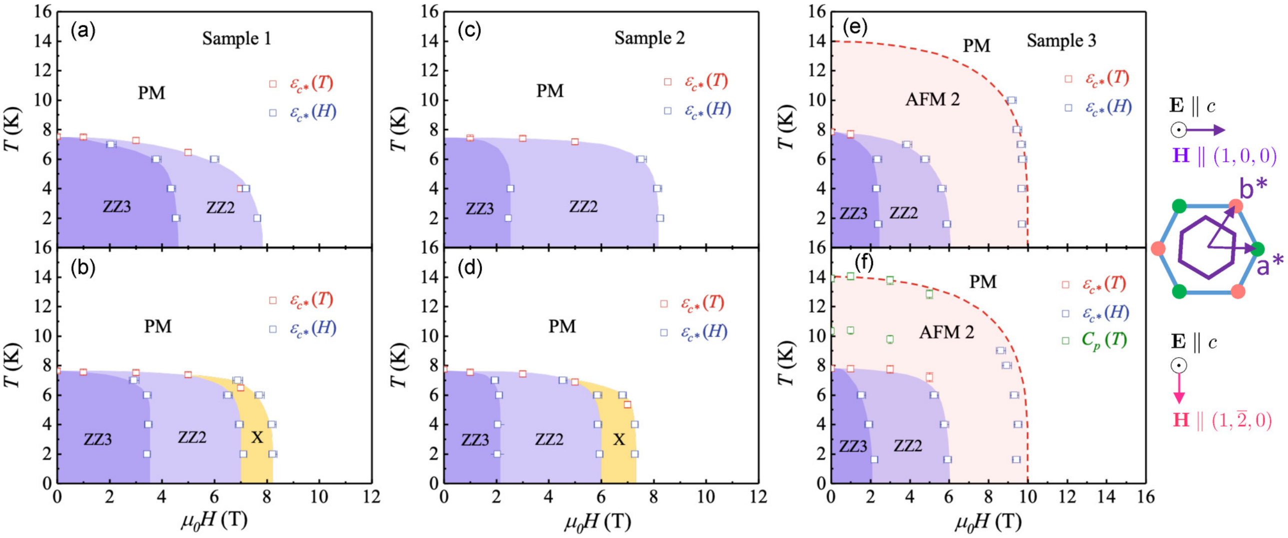

FIG. 5. T-H phase diagrams of the studied three samples derived from Figs. 2 and 4. (a) and (b) T-H phase diagrams of sample 1 with fields applied along $\mathbf{H} \parallel (1, 0, 0)$ and $\mathbf{H} \parallel (1, \bar{2}, 0)$, respectively. (c), (d) and (e), (f) Same representations to those of (a) and (b) for samples 2 and 3, respectively. The symbols ZZ3 and ZZ2 represent three and two domains in the zigzag phase, respectively. The field-induced intermediate state is labeled as the X phase. The paramagnetic state is labeled as PM and the zigzag AF order formed below T_{N2} is represented as AFM 2. Green squares were obtained in specific heat experiments.

techniques have been mapped out nicely using dielectric probing. Similarities can be found in samples 1 and 2 where the magnetic phase is mainly governed by the AF zigzag order formed below T_{N1}. Clear in-plane anisotropies are found for these two samples. For $\mathbf{H} \parallel (1, 0, 0)$, the main features take place at the domain repopulation field $\mu_0 H_r$ and the suppression of AF order crossing the $\mu_0 H_{c1}$ lines. An additional field-induced intermediate X state shows up between $\mu_0 H_x$ and $\mu_0 H_{c1}$ for $\mathbf{H} \parallel (1, \bar{2}, 0)$ in samples 1 and 2. Less anisotropy appears in sample 3 which has a sizable degree of stacking faults. Both transitions at $\mu_0 H_r$, $\mu_0 H_{c1}$, and $\mu_0 H_{c2}$ are identified, whereas the intermediate state is missing due to the collapse of $\mu_0 H_{c1}$ onto $\mu_0 H_x$. The stacking-fault-induced glassy phase of electric dipoles observed in samples 2 and 3 is not shown in the phase diagram, as it is not a long-range order. By comparing these three samples, it is clear that the ground state of α-RuCl$_3$ is very sensitive to structural details both in the magnetic and electric channels due to the strong interplay between lattice, spin, and charge degrees of freedom.

IV. CONCLUSIONS

In summary, we observe an out-of-plane dielectric anomaly in α-RuCl$_3$ which appears to be closely associated with inhomogeneously distributed stacking faults. This dielectric anomaly is a signature of a possible glassy state of local electric polarizations, which is evidenced by its strong frequency dependence and sizable dissipations. Immunity to strong external in-plane magnetic fields of this glassy state points to a structural origin instead of a magnetic root. Details of the magnetic phase diagram, including the domain repopulation, the field-induced intermediate state (field applied perpendicular to the Ru-Ru bonds), and the transition between AF ordered and disordered phases, were successfully mapped out using dielectric and magnetodielectric probing. The dielectric probing may thus serve as a promising tool for detecting stacking faults and studying the magnetic properties of α-RuCl$_3$ thin-film devices when bulk measurements are not accessible. Our findings also suggest that the ground state is rather fragile against structural perturbations both in the magnetic and electric channels. Further efforts are needed to overcome this difficulty and to eventually manipulate the novel Kitaev physics in α-RuCl$_3$-based devices.

ACKNOWLEDGMENTS

This work has been supported by the National Natural Science Foundation of China (Grants No. 11904040 and No. 12047564), Chongqing Research Program of Basic Research and Frontier Technology, China (Grant No. cstc2020jcyj-msxmX0263), Fundamental Research Funds for the Central Universities, China (Grants No. 2020CDJQY-A056, No. 2020CDJ-LHZZ-010, and No. 2020CDJQY-Z006), and Projects of President Foundation of Chongqing University, China (Grant No. 2019CDXZWL002). Y.C. acknowledges support by the National Natural Science Foundation of China (Grants No. 11674384 and No. 11974065). A.W. acknowledges support by the National Natural Science Foundation of China (Grant No. 12004056). L.Z. acknowledges support by the the National Natural Science Foundation of China (Grant No. 11874193) and Shenzhen Fundamental Research Fund for Distinguished Young Scholars (Grant No. RCJC20200714114435105).

---

[1] A. Kitaev, Ann. Phys. **321**, 2 (2006).

[2] C. Nayak, S. H. Simon, A. Stern, M. Freedman, and S. Das Sarma, Rev. Mod. Phys. **80**, 1083 (2008).

[3] C. Broholm, R. J. Cava, S. A. Kivelson, D. G. Nocera, M. R. Norman, and T. Senthil, Science **367**, eaay0668 (2020).

[4] S. Trebst, arXiv:1701.07056.

[5] J. Wen, S.-L. Yu, S. Li, W. Yu, and J.-X. Li, npj Quantum Mater. **4**, 12 (2019).

[6] Y. Singh, S. Manni, J. Reuther, T. Berlijn, R. Thomale, W. Ku, S. Trebst, and P. Gegenwart, Phys. Rev. Lett. **108**, 127203 (2012).

[7] K. A. Modic, T. E. Smidt, I. Kimchi, N. P. Breznay, A. Biffin, S. Choi, R. D. Johnson, R. Coldea, P. Watkins-Curry, G. T. McCandless, J. Y. Chan, F. Gandara, Z. Islam, A. Vishwanath, A. Shekhter, R. D. McDonald, and J. G. Analytis, Nat. Commun. **5**, 4203 (2014).

[8] I. Kimchi, J. G. Analytis, and A. Vishwanath, Phys. Rev. B **90**, 205126 (2014).

[9] T. Takayama, A. Kato, R. Dinnebier, J. Nuss, H. Kono, L. S. I. Veiga, G. Fabbris, D. Haskel, and H. Takagi, Phys. Rev. Lett. **114**, 077202 (2015).

[10] A. Glamazda, P. Lemmens, S. H. Do, Y. S. Choi, and K. Y. Choi, Nat. Commun. **7**, 12286 (2016).

[11] Y. Singh and P. Gegenwart, Phys. Rev. B **82**, 064412 (2010).

[12] A. Banerjee, C. A. Bridges, J. Q. Yan, A. A. Aczel, L. Li, M. B. Stone, G. E. Granroth, M. D. Lumsden, Y. Yiu, J. Knolle, S. Bhattacharjee, D. L. Kovrizhin, R. Moessner, D. A. Tennant, D. G. Mandrus, and S. E. Nagler, Nat. Mater. **15**, 733 (2016).

[13] H. B. Cao, A. Banerjee, J.-Q. Yan, C. A. Bridges, M. D. Lumsden, D. G. Mandrus, D. A. Tennant, B. C. Chakoumakos, and S. E. Nagler, Phys. Rev. B **93**, 134423 (2016).

[14] A. Glamazda, P. Lemmens, S.-H. Do, Y. S. Kwon, and K.-Y. Choi, Phys. Rev. B **95**, 174429 (2017).

[15] R. D. Johnson, S. C. Williams, A. A. Haghighirad, J. Singleton, V. Zapf, P. Manuel, I. I. Mazin, Y. Li, H. O. Jeschke, R. Valentí, and R. Coldea, Phys. Rev. B **92**, 235119 (2015).

[16] Y. Kubota, H. Tanaka, T. Ono, Y. Narumi, and K. Kindo, Phys. Rev. B **91**, 094422 (2015).

[17] S. Y. Park, S. H. Do, K. Y. Choi, D. Jang, T. H. Jang, J. Schefer, C. M. Wu, J. S. Gardner, J. M. S. Park, J. H. Park, and S. Ji, arXiv:1609.05690.

[18] Z. Wang, J. Guo, F. F. Tafti, A. Hegg, S. Sen, V. A. Sidorov, L. Wang, S. Cai, W. Yi, Y. Zhou, H. Wang, S. Zhang, K. Yang, A. Li, X. Li, Y. Li, J. Liu, Y. Shi, W. Ku, Q. Wu *et al.*, Phys. Rev. B **97**, 245149 (2018).

[19] S.-H. Baek, S.-H. Do, K.-Y. Choi, Y. S. Kwon, A. U. B. Wolter, S. Nishimoto, J. van den Brink, and B. Büchner, Phys. Rev. Lett. **119**, 037201 (2017).

[20] A. Banerjee, J. Yan, J. Knolle, C. A. Bridges, M. B. Stone, M. D. Lumsden, D. G. Mandrus, D. A. Tennant, R. Moessner, and S. E. Nagler, Science **356**, 1055 (2017).

[21] M. Majumder, M. Schmidt, H. Rosner, A. A. Tsirlin, H. Yasuoka, and M. Baenitz, Phys. Rev. B **91**, 180401 (2015).

[22] Y. Kasahara, T. Ohnishi, Y. Mizukami, O. Tanaka, S. Ma, K. Sugii, N. Kurita, H. Tanaka, J. Nasu, Y. Motome, T. Shibauchi, and Y. Matsuda, Nature (London) **559**, 227 (2018).

[23] M. R. Norman, Rev. Mod. Phys. **88**, 041002 (2016).

[24] Y. Zhou, K. Kanoda, and T.-K. Ng, Rev. Mod. Phys. **89**, 025003 (2017).

[25] Y. Cui, J. Zheng, K. Ran, J. Wen, Z.-X. Liu, B. Liu, W. Guo, and W. Yu, Phys. Rev. B **96**, 205147 (2017).

[26] M. He, X. Wang, L. Wang, F. Hardy, T. Wolf, P. Adelmann, T. Brückel, Y. Su, and C. Meingast, J. Phys.: Condens. Matter **30**, 385702 (2018).

[27] A. Banerjee, P. Lampen-Kelley, J. Knolle, C. Balz, A. A. Aczel, B. Winn, Y. Liu, D. Pajerowski, J. Yan, C. A. Bridges, A. T. Savici, B. C. Chakoumakos, M. D. Lumsden, D. A. Tennant, R. Moessner, D. G. Mandrus, and S. E. Nagler, npj Quantum Mater. **3**, 8 (2018).

[28] S. Gass, P. M. Cônsoli, V. Kocsis, L. T. Corredor, P. Lampen-Kelley, D. G. Mandrus, S. E. Nagler, L. Janssen, M. Vojta, B. Büchner, and A. U. B. Wolter, Phys. Rev. B **101**, 245158 (2020).

[29] C. Balz, P. Lampen-Kelley, A. Banerjee, J. Yan, Z. Lu, X. Hu, S. M. Yadav, Y. Takano, Y. Liu, D. A. Tennant, M. D. Lumsden, D. Mandrus, and S. E. Nagler, Phys. Rev. B **100**, 060405 (2019).

[30] P. Lampen-Kelley, L. Janssen, E. C. Andrade, S. Rachel, J. Q. Yan, C. Balz, D. G. Mandrus, S. E. Nagler, and M. Vojta, arXiv:1807.06192.

[31] K. Ran, J. Wang, W. Wang, Z.-Y. Dong, X. Ren, S. Bao, S. Li, Z. Ma, Y. Gan, Y. Zhang, J. T. Park, G. Deng, S. Danilkin, S.-L. Yu, J.-X. Li, and J. Wen, Phys. Rev. Lett. **118**, 107203 (2017).

[32] S.-H. Do, S.-Y. Park, J. Yoshitake, J. Nasu, Y. Motome, Y. S. Kwon, D. T. Adroja, D. J. Voneshen, K. Kim, T. H. Jang, J. H. Park, K.-Y. Choi, and S. Ji, Nat. Phys. **13**, 1079 (2017).

[33] C. Balz, L. Janssen, P. Lampen-Kelley, A. Banerjee, Y. Liu, J. Yan, D. Mandrus, M. Vojta, and S. E. Nagler, arXiv:2012.15258.

[34] H.-S. Kim and H.-Y. Kee, Phys. Rev. B **93**, 155143 (2016).

[35] S. Widmann, V. Tsurkan, D. A. Prishchenko, V. G. Mazurenko, A. A. Tsirlin, and A. Loidl, Phys. Rev. B **99**, 094415 (2019).

[36] S. Reschke, F. Mayr, S. Widmann, H.-A. K. von Nidda, V. Tsurkan, M. V. Eremin, S.-H. Do, K.-Y. Choi, Z. Wang, and A. Loidl, J. Phys.: Condens. Matter **30**, 475604 (2018).

[37] J. Zheng, Y. Cui, T. Li, K. Ran, J. Wen, and W. Yu, Sci. China-Phys. Mech. Astron. **61**, 057021 (2018).

[38] E. V. Stroganov and K. V. Ovchinnikov, Vestn. Leningr. Univ. Fiz. Khim. **12**, 152 (1957).

[39] T. Aoyama, Y. Hasegawa, S. Kimura, T. Kimura, and K. Ohgushi, Phys. Rev. B **95**, 245104 (2017).

[40] E. Courtens, Phys. Rev. Lett. **52**, 69 (1984).

[41] R. Bhowmik and R. Ranganathan, J. Magn. Magn. Mater. **248**, 101 (2002).

[42] A. A. Bokov and Z. G. Ye, J. Mater. Sci. **41**, 31 (2006).

[43] J. A. Sears, Y. Zhao, Z. Xu, J. W. Lynn, and Y.-J. Kim, Phys. Rev. B **95**, 180411 (2017).